Original Article

PINN-Based Tool Wear Modeling and Prediction

Zhang Yanping^{1,2*}, Kho Lee Chin¹, Wang Zhihan³, Zhang Mingqiang⁴, Yuan Dongfeng⁵

¹Faculty of Engineering, Universiti Malaysia Sarawak, Sarawak, Malaysia ²Shandong Provincial Key Laboratory of Industrial Big Data and Intelligent Manufacturing, Qilu Institute of Technology, Shandong, China. ³School of Information and Electrical Engineering, Shandong Jianzhu University, Shandong, China. ⁴School of Cyber Science and Engineering, Oufu Normal University, Shandong, China. ⁵School of QILU Transportation, Shandong University, Shandong, China.

*Corresponding Author: ypzhang@qlit.edu.cn

Received: 24 July 2025 Revised: 24 October 2025 Accepted: 03 November 2025 Published: 25 November 2025

Abstract - To address the challenges of low prediction accuracy and weak physical interpretability in tool wear modeling, this study proposes a Physics-Informed Neural Network (PINN)-based hybrid framework that integrates wear stage perception and physical prior knowledge. Four representative models-Long Short-Term Memory (LSTM), Stepwise Dual-Driven, Basquin-based PINN, and Empirical Formula-PINN (EF-PINN)-are constructed and systematically evaluated using real milling vibration datasets. The EF-PINN embeds empirical wear laws as soft physical constraints within the neural network loss function, enabling a balanced fusion of data-driven adaptability and physical interpretability. Experimental results demonstrate that EF-PINN achieves superior performance in wear trend fitting, nonlinear degradation modeling, and generalization under varying cutting conditions, significantly outperforming traditional data-driven and purely mechanism-based approaches. The main contributions of this work are: (1) Establishing a unified comparative framework for data-, hybrid-, and physics-informed models; (2) Developing an EF-PINN that bridges the gap between empirical knowledge and data-driven learning; and (3) Experimentally validating the effectiveness of integrating physical priors to enhance reliability and confidence. This study provides a new paradigm for high-precision, interpretable, and robust tool wear prediction in intelligent manufacturing.

Keywords - Tool Wear Prediction, PINN, LSTM, Basqui, Intelligent manufacturing.

1. Introduction

Milling cutters are core cutting components of highperformance CNC machine tools, and its wear state is directly related to the machining quality and manufacturing efficiency [1]. According to the statistics of the Metal Cutting Tool Technology Association of China Machinery Industry, failures caused by milling cutter wear account for approximately 75% of all CNC machine tool failures, while around 20% of total downtime originates from cutter damage [2, 3]. Therefore, accurate prediction of milling cutter wear is essential to enhance tool utilization, ensure machining stability, and reduce production costs [4].

However, directly predicting cutter wear from raw multisensor signals remains highly challenging, as it is necessary to extract effective and wear-sensitive features through advanced signal processing methods to establish the correlation between sensor data and tool degradation. Although data-driven models such as deep neural networks [5, 6] have demonstrated remarkable performance under complex operating conditions, they suffer from several limitations: (1) Strong dependence on large volumes of high-quality labeled data, which are often difficult and costly to obtain in industrial environments; (2) Poor interpretability and weak physical consistency, leading to limited generalization capability across varying cutting conditions and small-sample scenarios.

To address these challenges, PINN [7, 8] has recently emerged as a promising paradigm, integrating physical constraints into neural network architectures or loss functions to achieve a hybrid fusion of physical interpretability and data adaptability. Despite the success of PINN in various scientific and engineering fields, the application of PINN in tool wear modeling remains underexplored and fragmented.

Current research gaps can be summarized as follows:

- Most existing models focus on isolated physical mechanisms or single operating conditions, lacking systematic comparative analyses among different physics-data fusion strategies.
- The applicability and robustness of PINN under realistic milling conditions, characterized by nonlinear wear processes, time-varying cutting parameters, and multisource signal interference, remain insufficiently



validated.

 Few studies have addressed the challenges of dynamic multi-physical field coupling (mechanical-thermalchemical), transient boundary conditions, and cross-scale damage evolution, which are critical for achieving highaccuracy and real-time tool wear prediction in industrial applications.

In this study, an EF-PINN model is proposed, which innovatively integrates empirical wear laws into the neural network structure and loss function to achieve a balanced fusion of data-driven adaptability and physical interpretability. A unified experimental evaluation framework based on vibration signal analysis is also established to systematically investigate the capability of EF-PINN in industrial tool wear prediction under complex service conditions.

Unlike traditional deep learning models that rely solely on statistical correlations or existing PINN frameworks that are constrained by specific physical formulations, the proposed EF-PINN introduces empirical wear equations as soft physical constraints, enabling the model to capture both macroscopic wear evolution and microscopic degradation dynamics. This design enhances the model's generalization ability across varying cutting parameters and small-sample scenarios, providing improved stability and physical consistency compared with conventional LSTM, dual-drive, and standard PINN models. Experimental validation using real-world production data demonstrates that the EF-PINN framework effectively mitigates limitations in multi-field coupling and transient boundary modeling. This study provides new theoretical insights and engineering guidance for developing cross-platform, multi-source information fusion models for intelligent tool wear monitoring and prediction.

2. Related Work

Feature extraction not only helps to eliminate redundant information and reduce computational complexity, but also directly affects the accuracy of wear prediction. In recent years, many researchers have proposed effective methods for feature extraction and wear modelling. In terms of data-driven modelling, Guo et al. [9] constructed a pyramid LSTM selfencoder to achieve efficient wear prediction through spectral compression; Cheng et al. [10] combined feature normalization, attention mechanism, and BiLSTM-CNN network to improve the robustness of multistep prediction; Zhang et al. [11] applied the fusion of SCINet and Isolated Forest to the RUL prediction of bearings to improve the model accuracy and stability; Li et al. [12] optimized LSTM by combining sideband energy ratio and tree seeding sub algorithm to achieve the identification of degradation process of wind turbine main bearing. It has been shown that the integration of physical knowledge can effectively improve the accuracy and stability of tool wear prediction models: Yuan et al. [13] integrated multiple physical information to construct a fusion model, and achieved more accurate and consistent wear prediction under unknown working conditions; Li et al. [14] optimized the network structure based on cutting mechanics and wear mechanism, and pre-trained the network with largescale simulation data, which effectively alleviated the problem of data shortage; Yuan etc. problem; Yuan et al.[15] proposed an online prediction framework based on SSAE and physical knowledge assistance, and improved the accuracy and adaptability by dynamically updating the model; Liu et al. [16] constructed a regularization-based sensor modelling framework, TCMoR, and mined the physical features of machining process through frequency domain features; Deng et al. [17] combined particle filtering to enhance the accuracy of physical simulation, and constructed a Physical Information Bayes Deep Dual Network (PI-BDDN) to enhance the feature extraction capability.

Regarding Structural Innovation, Liu et al. [18] proposed a PIS-ETN network and designed a texture digital twin module with a knowledge embedding mechanism to achieve deep fusion of processing parameters and sensor data; Fang et al. [19] proposed a TWM dual knowledge embedding model, which introduces physical constraints and data augmentation strategies to effectively improve real-time performance and prediction accuracy; Zhang et al. [20] systematically reviewed the research lineage of physics-data fusion modelling and summarized the development trend of the TWM field. For fault diagnosis and small-sample learning, Gao et al. [21] proposed MPINet multiscale network and introduced Physical Information Blocks (PIB) for finer feature extraction; Kim et al. [22] designed a model that fuses time-frequency multidomain and attention mechanisms to effectively improve the fault recognition performance in noisy environments; Li et al. [23] fused physical modelling with meta-learning to improve the cross-wear rate through empirical model fitting with physical constraint embedding to enhance the adaptability across wear rate conditions. Chen Chong et al. [24] reviewed the development paths and challenges of physics-guided deep learning from a theoretical perspective, highlighting its application in scientific and engineering problems. Furthermore, to balance the trade-off between accuracy and stability in state prediction of key manufacturing components, J. Hua et al. [25] proposed a PINN Weight Learning. This approach quantifies the confidence of both physical and data-driven models via variance and achieves adaptive fusion between them, effectively suppressing noise interference and improving generalization performance.

3. Theoretical Foundations

3.1. Tool Wear Mechanism and Evolutionary Stage

During the metal cutting process, intense contact between the tool and the workpiece occurs at high temperature, high pressure, and high speed, resulting in physical/chemical behaviours such as plastic deformation, diffusion, oxidation, and abrasive wear of the tool material. As listed in Table 1, tool wear shows a typical three-stage evolutionary pattern, and in each stage, the characteristics of vibration signals are different.

- Initial wear stage: The tool contact surface quickly establishes contact with the workpiece, the rough microconvex body at the tip of the tool is gradually smoothed, and the VB value increases rapidly. The wear rate in this stage is high, but the duration is short.
- 2. Stable wear stage: After forming a stable contact surface, the wear tends to be regular, the VB value increases at a nearly linear rate, and the wear rate is the most stable, which is the focus of predictive modelling.
- 3. Intense wear stage: In the pre-failure stage of the tool, the wear is suddenly accelerated, and the VB value shows an exponential increase, accompanied by boundary breakage, micro crack expansion, and other violent failure characteristics.

| Table 1. Characteristics of vibration signals in different phases |
|---|
|---|

| Stage | Vibration Amplitude | High Frequency Component | Envelop Energy | Description |
|-----------------------|---|-----------------------------|----------------------------|--|
| Initial Wear Lower | fluctuating Less | less | Inconspicuous | Pronounced Surface still smooth, little interference |
| Steady Wear | Steady growth | Marked increase | Gradual increase in energy | Contact increases, friction becomes intense |
| Intensive Wear | Significant fluctuations, frequent pulses | Peaks are significant | local mutation | Knife spalling, destabilization shocks |

3.2. LSTM

LSTM represents an enhanced variant of recurrent neural networks, which employs gating mechanisms to regulate the addition or removal of information. Its cumulative structure facilitates more efficient derivative computation during backpropagation, thus alleviating the vanishing gradient issue and allowing the network to learn long-term dependencies over extended sequences. The LSTM architecture primarily comprises an input gate r_t , output gate o_t , forget gate f_t , and memory $\operatorname{cell} c_t$. Among them, i_t it determines the information to be saved or updated at the current time, f_t decides which information to discard and which to retain, and also avoids the gradient vanishing and gradient explosion problems caused by iteration in some way, and ot determines the amount of information input to the memory cell, while the memory cell c_t contains the information it stores at a given time t. The formula utilized for updating the state of each gate and unit is defined as follows:

$$r_{t} = \sigma(W_{i} * [h_{t-1}, x_{t}] + b_{i})$$
(1)

$$f_{t} = \sigma(W_{f} * [h_{t-1}, x_{t}] + b_{f})$$
 (2)

$$c_{t} = f_{t} * c_{t-1} + i_{t} * \tanh(W_{c} * [h_{t-1}, x_{t}] + b_{c})$$
(3)

$$o_{\cdot} = \sigma(W_{\circ} * [h_{\cdot, \cdot}, x_{\cdot}] + b_{\circ}) \tag{4}$$

$$h_{c} = o_{c} * \tanh(c_{c}) \tag{5}$$

In LSTM networks, the cell state preserves long-term memory, while the input gate and forget gate facilitate the

network's autonomous learning of which information to retain or discard, rendering it particularly adept at processing lengthy sequential data. The architectural design of LSTM enables the network to adaptively process and preserve critical information through its gating mechanisms, thereby optimizing the handling of time series data.

3.3. PINN

PINN enhances the model's generalization and prediction accuracy by incorporating physical laws (such as differential equations and boundary conditions) directly into the neural network's loss function, ensuring that the model not only fits the data but also adheres to the underlying physical constraints during training. In tool wear prediction, PINN combines wear mechanism models and sensor data to achieve accurate prediction of wear states. The empirical tool wear-time model developed by Sipos [26] is employed, which predicts tool wear over time based on specified cutting speed, feed rate, and depth of cut. Its equation is:

$$x(t_c) = t_c \exp(A + Bt_c + Ct_c^2) \tag{6}$$

$$f(x; \frac{\partial u}{\partial x_1}, \dots, \frac{\partial u}{\partial x_d}; \frac{\partial^2 u}{\partial x_1 \partial x_1}, \dots, \frac{\partial^2 u}{\partial x_1 \partial x_d}; \dots; \lambda) = 0$$
 (7)

In this context A,B, and C represent empirical parameters derived from experimental data, u denote the wear value, t signifies time, and x constitutes the parameter matrix composed of tool parameters. The numerical differentiation at time t is computed to determine the error between the calculated values and the physical formula.

$$\frac{du}{dt} - c_1(1 + bt + 2c_2t^2) \exp(a + bt + c_2t^2) = 0$$
 (8)

The constants a, b, c_1 and c_2 are derived from experimental data.

3.3.1. PINN based on the Basquin Fatigue Formulation

The applicability of Basquin's law to tool wear is supported by several key factors. First, both fatigue failure and tool wear share the same microscopic damage mechanism, involving dislocation accumulation followed by microcrack initiation and propagation. Second, the cutting process imposes high-frequency cyclic mechanical loads on the tool, analogous to high-cycle fatigue conditions. Third, the presence of cutting heat introduces a thermal-mechanical coupling effect, which further amplifies fatigue damage. Lastly, experimental observations reveal strong correlations between tool wear and fatigue phenomena, as evidenced by fatigue-like features on worn tool surfaces. These factors collectively justify the use of Basquin's law as a valid framework for describing tool wear behavior. This cross-scale physical correlation provides a solid scientific foundation for wear prediction based on fatigue theory and has unique advantages in explaining the tool life under variable operating conditions. The Basquin fatigue model is a typical stress-life empirical formulation:

$$N = C * \Delta s^m \tag{9}$$

Where N denotes the number of life cycles, Δs denotes the stress amplitude, C and m denotes the constants fitted to the experimental data. In PINN, the Basquin formula is embedded as a physical constraint in the network structure, and the implementation includes:

Network Structure

The base network consists of three fully connected layers with input and output dimensions of (2, 63), (63, 63), and (63, 63). The physical information network consists of two fully connected layers with dimensions (63, 21) and (21, 21). The

network contains a ReLU activation function, a Dropout layer (with a dropout rate of 0.3), and a BatchNorm1d layer for preventing overfitting and accelerating training.

Forward propagation

The input data is initially processed by the base network layer to extract features, which are subsequently passed into the physical information network to compute the physical layer output according to whether the Basquin physical constraints are enabled or not. Finally, the physical layer output is combined with the base network output to get the prediction result through the final fully connected layer.

3.3.2. PINN based on Empirical Formula

This method combines the ideas of data-driven and physical knowledge embedding by firstly modelling the vibration signals during the milling process using an LSTM network, and extracting the wear evolution features from the time-series data.

At the same time, the empirical formulation provided by Equation (6) is utilized as a physical a priori to impose physical consistency constraints on the network outputs, guiding the model to better capture the key dynamics at each stage of the wear process. By fusing the data features with the knowledge of the wear mechanism, the model's understanding of the wear evolution laws and prediction accuracy are improved.

4. Design and Implementation of PINN Model based on Empirical Formula

The architecture of the empirical formula-based PINN model is shown in Figure 1 and consists of three parts: data-driven model, physics-driven model, data loss, and optimization.

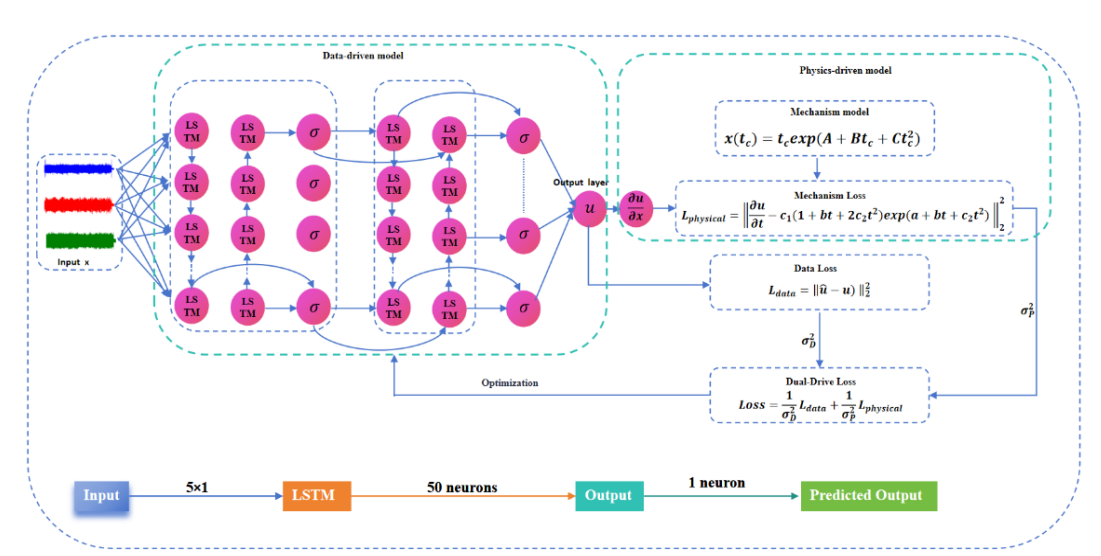


Fig. 1 Data physical dual driver model architecture

4.1. Input Layer

The input data x is used as a vibration signal in three axes. Firstly, the original data x is subjected to data cleaning to remove nulls, outliers, and duplicates, and the missing data are filled in using mean value interpolation. Secondly, the signal denoising is performed using the wavelet method; finally, it is entered into the LSTM for training after using a normalization process and sliding window slicing.

4.2. Data-Driven Model

To achieve accurate prediction of tool wear trends, a datadriven approach based on a time series deep learning model is adopted. The model utilizes an LSTM neural network to capture temporal dependencies in the tool wear data. Specifically, the input to the model is a sequence of five consecutive wear values (i.e., sliding window length or look_back = 5), and the output is the predicted wear value at the next time step.

The LSTM-based prediction model is structured with an LSTM layer for sequence feature extraction, followed by a fully connected layer and an output layer to produce regression outputs. The network architecture and training configuration are described in detail in Section 4.2.

In terms of training setup, the data set is divided into a training set and a test set in a ratio of 8:2. The model is trained for 100 epochs using a batch size of 16. The Adam optimizer is employed with its default learning rate of 0.001, which facilitates adaptive learning in the presence of non-stationary time series. The initial wear value is normalized, and the model outputs continuous wear predictions to support wear trend tracking and decision-making in tool life management.

4.3. Physically Driven Model

The physical component involves computing the temporal error between the numerically derived differential equations and the physical formulas obtained through derivation. The parameters of the differential equation are denoted by $\lambda = (a, b, c_1, c_2)$. To constrain the solution space of the neural network, the tool wear mechanism is incorporated into the model's loss function as a regularization term.

$$L_{physical} = \left\| f(x; \frac{\partial u}{\partial x_1}, \dots, \frac{\partial u}{\partial x_d}; \frac{\partial^2 u}{\partial x_1 \partial x_1}, \dots, \frac{\partial^2 u}{\partial x_1 \partial x_d}; \dots; \lambda) \right\|_{2}$$

$$= \left\| \frac{\partial u}{\partial t} - c_1 (1 + bt + 2c_2 t^2) \exp(a + bt + c_2 t^2) \right\|_{2}^{2}$$
(10)

4.4. Loss Function

Data Loss Function:

$$L_{data} = \left\| \hat{u} - u \right\|_{2}^{2} \tag{11}$$

In the equation, \hat{u} represents the predicted value of tool wear in the data network segment, while u denotes the measured value of tool wear.

The total loss function is defined as:

$$Loss = L_{physical} + L_{data} \tag{12}$$

To maximize the respective roles of data and physical components, a weighted mechanism is introduced into the loss function through variance calculation:

$$E[(\varepsilon - \overline{\varepsilon})] = \frac{1}{d} \sum_{i=1}^{d} (\varepsilon - \overline{\varepsilon})^{2}$$
(13)

$$\sigma^2 = E[(\varepsilon - \overline{\varepsilon})^2] \tag{14}$$

The variances predicted by data-driven and mechanism-based approaches are utilized to form their respective reciprocals as dynamic weights. These weights are subsequently incorporated into the dynamic weighting of the loss function after a specified number of training epochs, thereby enabling the appropriate adjustment of the proportion between data-driven and mechanism-based components. This ensures that the model maintains a balanced consideration of data fitting and physical constraints across various operational conditions. Heregrepresents the predicted error and $\overline{\epsilon}$ denotes the expected error of the models. Ultimately, based on the weight allocation strategy, the loss function is defined as follows:

$$Loss(W; \lambda) = \frac{1}{\sigma_{o}^{2}} L_{data} + \frac{1}{\sigma_{o}^{2}} L_{physical}$$
 (15)

The training process aims to find the optimal weights W by minimizing the loss function $Loss(W; \lambda)$ through gradient-based optimization. Since the physical model parameters λ are unknown in tool wear prediction, the PINN framework simultaneously learns both W and λ , expressed as $W^*, \lambda^* = argmin_{W,\lambda} Loss(W; \lambda)$.

5. Experimental Verification

5.1. Test Platform and Data Acquisition

5.1.1. Test Platform

In this study, a tool wear testing platform is established to acquire vibration signals and measure tool wear values throughout the entire tool life cycle. In this paper, a tool wear test platform is constructed for tool full life cycle vibration signal acquisition and tool wear value measurement. The workpiece milling process is carried out on a CNC machine vertical machining center (VDF-850), as illustrated in Figure 2. The cutting tool used is a three-flute end mill with a

diameter of 10 mm, and the workpiece material is 45# steel in a cylindrical form. A KS903 vibration sensor was employed to capture vibration signals from the CNC spindle along the X, Y, and Z axes at a sampling frequency of 10,240 Hz. To accelerate the wear process, dry milling was performed

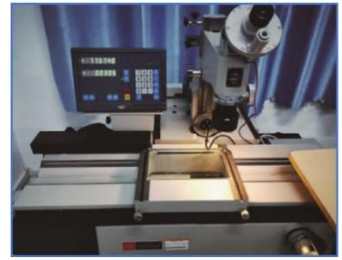
without the use of cutting fluid. The machining continued until the tool exhibited severe wear, and minor chipping appeared on the cutting edge. 35-47 sets of test data were collected for each tool, and each milling process took. The detailed experimental parameters are listed in Table 2.



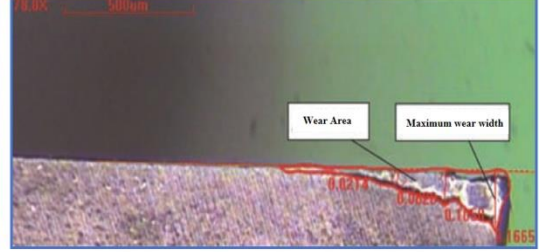
(a) Vertical Machining Center VDF-850



(b) Wear diagram of the main cutting edge



(c) 19JC Digital Universal Tool Microscope



(d) Flank wear pattern of the secondary cutting edge

Fig. 2 Tool wear test platform

Table 2. Parameters of machining process conditions for tool wear test platforms

| Parameter Name | Model/Value | Parameter Name | Model/Value |
|-----------------------|---------------------------|-------------------------|-----------------------------|
| CNC | Vertical Machining Center | Spindle speed/(r/min) | 2548 |
| CNC | VDF-850 | Spindle speed/(I/IIIII) | 4140 |
| Tool | Triple-flute end mill | Feed rate/(mm/min) | 764.4 |
| | Φ10 (D10*25*75*3F) | reed rate/(mm/mm) | 1242 |
| Vibration Sensors | KS903 | Back draft/mm | 0.5 |
| data acquisition card | WebDAQ-504 | Milling width/mm | 2 |
| Workpiece materials | No. 45 Steel | Milling depth/mm | 5 |
| Workpiece | 90 | Wear value collection | 19JC Digital Universal Tool |
| Diameter/mm | 160 | instruments | Microscope |

5.1.2. Measurement and Labeling of Cutter Wear Value Classification

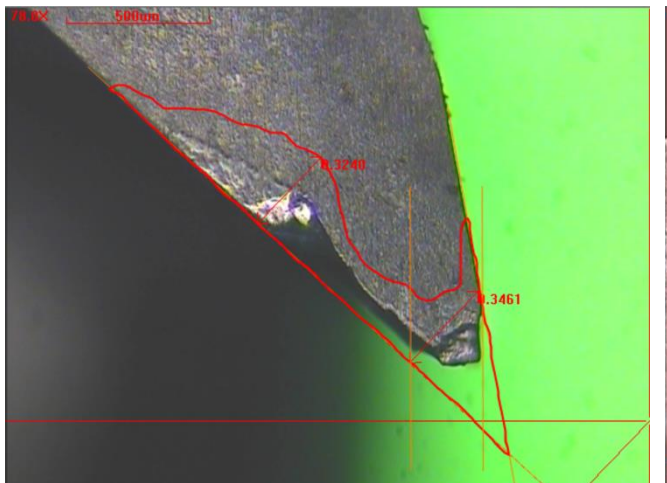
An end mill is the most commonly used type of milling cutter in CNC milling, and edge deformation or damage gradually forms due to the interaction between the end mill and the workpiece. According to the end mill life test standard of national standard GB/T 16460-2016 [27], it is known that the width value of the wear band of the back face is the most commonly used wear criterion. At the same time, in many academic materials, most of the tools refer to face VB as the tool wear standard and tool change basis [28]. In this paper, through the 19JC digital universal tool microscope (as shown in Figure 3(b) to measure each milling tool after the main rear face of the maximum VB value, the main rear face of the

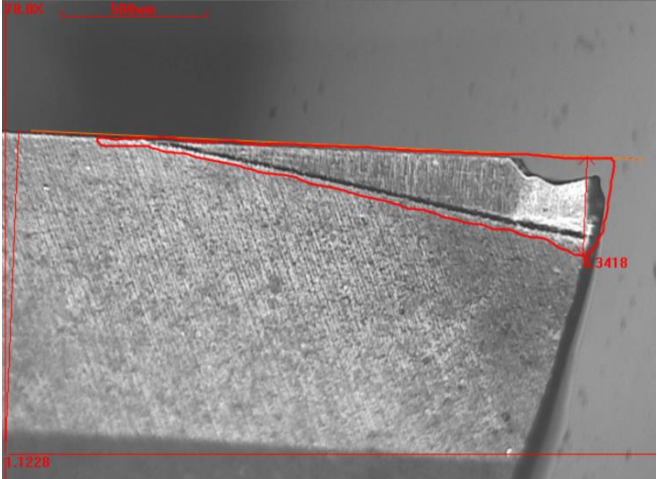
 $1/2a_p$ back draft at the VB value, the main rear face of the S_{VB} value, the vice rear face of the maximum VB value, the vice rear face of the S_{VB} value (in which the VB represents the back of the width of the wear, the S_{VB} represents the area of the wear) and other labels as a basis for the different stages of tool wear for the labeling. This is the basis for labeling at different stages of tool wear.

In the experiment, the sampling frequency of the vibration signal was determined based on the sampling theorem. The sampling frequency was set to 10kHz, and two sampling durations were used: when the spindle speed was 2548 r/min, each sampling lasted 4'35". When the spindle speed is 4140 r/min, each sampling lasted 2'28". The vibration sensor

recorded acceleration signals along the X, Y, and Z directions. After data acquisition, the cutting tools were removed, and their wear values were measured using a digital universal tool microscope. The recorded parameters included the maximum VB and the VB value at $1/2a_p$ the primary and rear tool faces, as well as the S_{VB} value of these faces, followed by the

maximum VB value of the secondary and rear tool faces, and the S_{VB} value of the secondary and rear tool faces. The wear widths of the main rear face and the secondary rear face of the third edge of Tool No. 1 measured 33rd are marked as shown in Figure 3, and the wear area is the closed cloud line area of the wear zone in the figure.





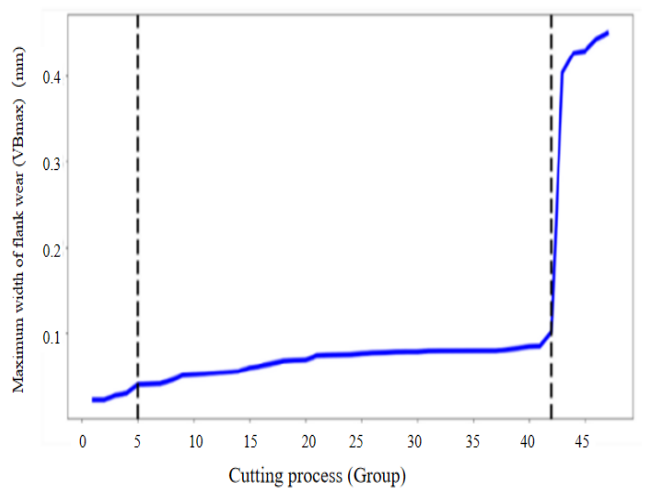
(a) Primary flank wear on the first cutting edge

(b) Wear observed on the first flank of the secondary cutting edge

Fig. 3 Data acquisition pictures of the tool under the universal tool microscope

The maximum wear width values for the full life cycle of the tool are shown in Figure 3(b), with the VB max value for the 1st edge of tool No. 3 as an example. As can be seen from the figure, the tool wears faster in the initial stage, and the slope of the wear curve is larger in this stage. In the steady state wear stage, the wear value grows uniformly until it reaches the limit value, and this stage is the effective working time of the tool. In the sharp wear phase, the tool wear value increases rapidly, leading to tool failure, and the slope of the wear curve increases rapidly in this phase. Although the initial wear stage is not very obvious in Figure 6, in the vibration signal time-domain diagram in Figure 7, the amplitude of the

vibration signal is larger in the initial stage, and then it rapidly enters the steady state wear stage, which is produced because the Surface of the new tool is rough and uneven, and the contact stress is larger, and at the same time, there is a decarburization of the new tool, and surface defects caused by the oxidized layer. After the tool enters the steady state wear stage, the vibration signal amplitude increases slightly and remains stable. Finally, the vibration signal amplitude gradually increases when it is about to enter the rapid wear stage. Therefore, combining Figures 4-5, the vibration signal data set is categorized into three categories in this paper, corresponding to three different tool wear stages.





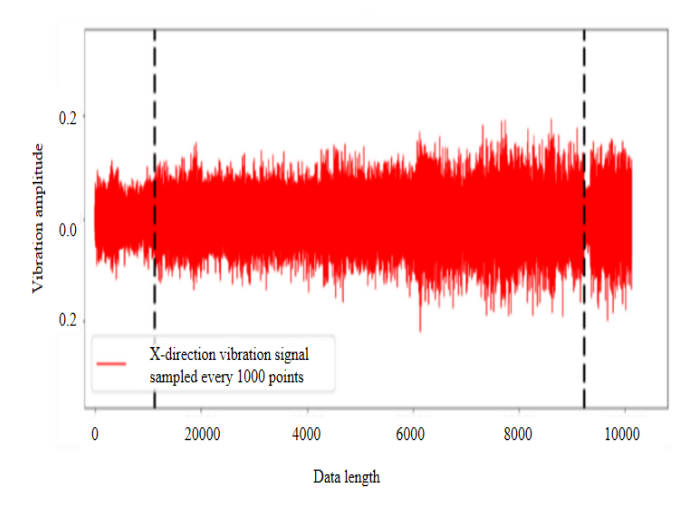


Fig. 5 Time domain plot of the full life cycle vibration signal in the X direction of the tool

5.1.3. Open Data Set

The SDU-QIT End Milling Cutter Accelerated Life Test Dataset was employed in this study. The data set was collected from surface milling experiments using five new tools, resulting in over 50 GB of multi-sensor data covering the entire tool life cycle. It contains the full life cycle vibration signals of each end mill and is clearly labeled with various labels such as maximum wear width VB, wear width at $1/2a_p$ (back draft), wear area S_{VB} , and maximum wear width and wear area S_{VB} on the secondary back of each tool.

The data set has been publicly released at "https://www.qlit.edu.cn/datasets/". In this paper, the wear data collected from tools No. 4 and No. 5 were employed for model training and evaluation, with the data split into training and validation sets at a 7:3 ratio.

5.2. LSTM Network Structure

5.2.1. Model Structure Design

Network Hierarchical Structure: This model adopts a single-layer LSTM structure, constructed using the method model. Add (LSTM(...)). Its purpose is to capture the long-term dependency features in time series. The structure is simple, facilitating debugging and training.

Number of Hidden Units

The LSTM layer contains 50 neurons, denoted as LSTM (50), which is used to enhance the feature extraction ability for sequential data.

Time Step (Sequence Length)

The look_back parameter is set to 5, meaning that the model inputs data from 5 time steps each time, which helps to extract the short-term dynamic features in the time series.

Regularization Strategy

This model does not employ the Dropout mechanism. There is no explicit addition of a Dropout layer or setting of the dropout parameter. Therefore, the model is relatively sensitive to changes in the training data.

Output Layer Design

A single-neuron fully connected layer, Dense (1), is used as the output layer, which is suitable for scalar prediction in regression tasks.

Input Dimension

The input shape of the model is (5,1), indicating that each sample contains 5 time steps, with 1 feature quantity at each time step.

5.2.2. Training Configuration Parameters

Batch Size

During the training process, a batch size of 16 is adopted, which represents a better choice when balancing the training speed and stability.

Optimizer and Learning Rate

The Adam optimizer is employed with its default learning rate of 0.001, and is adopted without manual tuning. Its adaptive adjustment capability is particularly effective for non-stationary sequential data.

Number of Training Epochs

The training process is conducted for 100 epochs to ensure that the model adequately captures the temporal characteristics present in the data.

Validation Set Setup

A static partitioning strategy is adopted. 20% of the original data is used as the test set, and during the training phase, it is used as the validation set in the form of 'validation data=(X test, y test)'.

Data Partitioning Ratio

The partitioning ratio between the training set and the test set is 8:2, which is achieved through 'train_size = int(len(X)*0.8),' facilitating the verification of the model's generalization performance.

5.2.3. Selection of Loss Weight Coefficients

To ensure a balanced contribution between the data-driven loss and the mechanism-constrained loss, the initial weights are set equally (0.5). As training progresses and the model enters a stable phase, an adaptive weighting strategy is employed to dynamically adjust the contributions of each loss component, based on both statistical variance and gradient-based feedback. Specifically, the combined loss function adopted in Section 3.3 (see Equation (15)) incorporates the inverse of the predicted error variances from the data-driven and physics-informed components as dynamic weighting coefficients. This variance-based formulation allows the model to account for the relative uncertainty in each submodel, ensuring that the more stable component exerts a greater influence on the overall loss optimization.

In addition, the model monitors the gradient magnitudes of each loss term during training. Larger gradients typically indicate a more substantial prediction error, and the associated weight is correspondingly increased. This gradient-aware adjustment mechanism enhances the model's responsiveness to dominant sources of error and improves convergence behavior. By jointly considering both the variance-based and gradient-based dynamics in the loss weighting process, the model maintains a balanced trade-off between empirical accuracy and physical consistency, contributing to improved robustness and generalization across varying operating conditions.

5.3. Experimental Results

The traditional data-driven model (LSTM), the Basquin-PINN, and the EF-PINN are considered in this work. In order to comprehensively evaluate the performance of each model in the tool wear prediction task, this paper selects five indexes, namely, Mean Absolute Error (MAE), Mean Square Error (MSE), Root Mean Square Error (RMSE), Coefficient of

Determination (R^2 R²), and Mean Absolute Percentage Error (MAPE). The experimental results on the tools No. 4 and No. 5 datasets are shown in Table 3.

Table 3. Model-specific experimental results

| | Tool 4: Experimen | ital results across different mod | lels |
|---------------------------|-------------------|-----------------------------------|---------|
| Evaluation Metrics | LSTM | Basquin-PINN | EF-PINN |
| MAE | 0.7498 | 0.4474 | 0.0840 |
| MSE | 1.1702 | 0.3319 | 0.0272 |
| RMSE | 1.0818 | 0.5761 | 0.1651 |
| \mathbb{R}^2 | 0.6428 | 0.9480 | 0.9917 |
| MAPE | 1.10% | 0.66% | 0.13% |
| | Tool 5 Experimen | tal results across different mod | lels |
| Evaluation Metrics | LSTM | Basquin-PINN | EF-PINN |
| MAE | 1.0862 | 2.2934 | 0.0341 |
| MSE | 1.4138 | 5.528 | 0.0020 |
| RMSE | 1.1890 | 2.3511 | 0.0449 |
| \mathbb{R}^2 | 0.7997 | 0.3586 | 0.9997 |
| MAPE | 1.66% | 3.57% | 0.05% |

5.3.1. Analysis of the Experimental Results for Tool No. 4

On the No. 4 knife data set, the tool stage division PINN model has the best performance in all indicators, with MAE, MSE, and RMSE of 0.0840, 0.0272, and 0.1651, respectively, which are significantly lower than those of other models, indicating that it has a significant advantage in error control. Meanwhile, the R² value of the decision system of the model is as high as 0.9917, which fully indicates that it can accurately portray the nonlinear evolution process of tool wear with strong fitting ability. In addition, the MAPE is only 0.13%. with a very small relative error, which further verifies the dual advantages of the model in terms of accuracy and stability. In contrast, although the traditional LSTM model performs relatively well in the benchmark data-driven model (R^2 = 0.6428), it is significantly inferior to the stage-divided PINN in terms of the error metrics, and the MAPE is high, with limited generalization ability. Basquin PINN achieves a fitting ability $R^2 = 0.9480$ due to the inclusion of physical priors; however, it still suffers from cumulative errors, suggesting that a single physical equation is insufficient to model complex multi-stage wear behavior. The step-by-step dualdrive model has the worst performance in each index, indicating that its physical and data fusion mechanism needs to be further optimized to adapt to the changing characteristics of the dynamic wear process.

5.3.2. Analysis of the Experimental Results of Tool No. 5

In the No. 5 knife data validation, the tool stage division PINN model still shows leading prediction performance. Its *MAE*, *MSE*, and *RMSE* are 0.0341, 0.0020, and 0.0449, respectively, and a R^2 value of 0.9997, which are all superior to those of the traditional LSTM ($R^2 = 0.7997$) and Basquin PINN ($R^2 = 0.3586$). This indicates that the proposed model maintains strong stability and robustness under complex wear conditions. It is worth noting that the performance of the

Basquin PINN model decreases dramatically on this data set, with the RMSE and MAPE rising to 2.3511 and 3.57%, respectively, reflecting that it is difficult for a single fatigue equation to accurately characterize the multi-stage nonlinear change rule in the actual wear process.

5.3.3. Comprehensive Analysis and Comparison with Existing Studies

Combining the experimental results of both Tool No. 4 and Tool No.5 datasets, the stage-divided PINN model significantly outperforms the other comparative models in a number of indicators. By introducing wear-mechanism-based physical constraints and a stage-aware structural prior, structural prior, the model enhances its nonlinear modeling capability and generalization across different wear stages, achieving both high accuracy and stability. Compared with existing studies, the superiority of the proposed model is further highlighted. For instance, the Physics-Informed Meta Learning (PIML) model proposed in [23] reports RMSE =3.17 and MAE = 1.95 in the x-direction, while the Physics-Assisted Online Learning model in [15] (combining SSAE feature extraction and MLP prediction) achieves an average MSE of 42.0069. The PINN-WL model in [25] yields lower MAE values (0.04 on the Ideahouse data set and 0.05 on the NASA data set) but under idealized and small-scale benchmark conditions. In contrast, our stage-divided PINN achieves RMSE = 0.1761 and MAPE = 0.15% on real industrial milling datasets, demonstrating superior precision and stronger generalization in complex, variable-load environments. Similarly, the SPRes-BiGRU hybrid model in [19] attains an average MSE of 9.10 on the PHM2010 dataset, which remains significantly higher than that of our model, indicating that embedding wear-stage priors within the PINN structure effectively enhances cross-condition adaptability and interpretability. Overall, the proposed stage-divided PINN framework provides a new physics-data integration paradigm that surpasses existing PINN and hybrid models in both quantitative accuracy and physical reliability, making it particularly suitable for intelligent manufacturing scenarios characterized by multi-stage, dynamically evolving wear processes.

5.4. Experimental Results and Visualization Analysis 5.4.1. Analysis of Tool No. 4 Prediction Results Analysis of LSTM Model Prediction Results

As shown in Figure 6, the LSTM model exhibits a generally correct trend in predicting the tool wear evolution, with the predicted wear (orange line) following the real wear (black line) across most samples. However, noticeable deviations can be observed at the look-back samples 0-1 and 3-4, where the absolute error (blue line) increases significantly. This indicates that the LSTM model has limited capability in accurately capturing the nonlinear variations in the wear process, especially during transitional and rapid wear phases.

Overall, while the LSTM model can learn the general wear trend, its prediction accuracy decreases when the wear dynamics become more complex, resulting in accumulated errors and insufficient robustness under varying operating conditions.

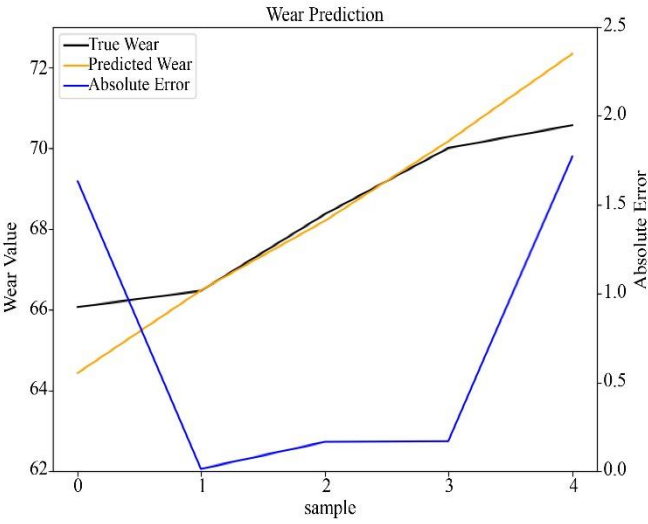


Fig. 6 Traditional neural network LSTM

Analysis of prediction Results based on the Basquin-PINN Model

Considering the potential contribution of physical prior to the modeling accuracy, this paper further constructs a physically guided neural network model (Basquin-PINN) based on Basquin's fatigue damage theory, as shown in Figure 7. The model guides the network to learn wear patterns by embedding physical constraints. However, the experimental results show that its prediction accuracy fails to meet expectations, mainly because the model's high dependence on physical constraints inhibits its ability to learn data features autonomously to a certain extent, thus limiting its adaptability and generalization ability in complex wear scenarios.

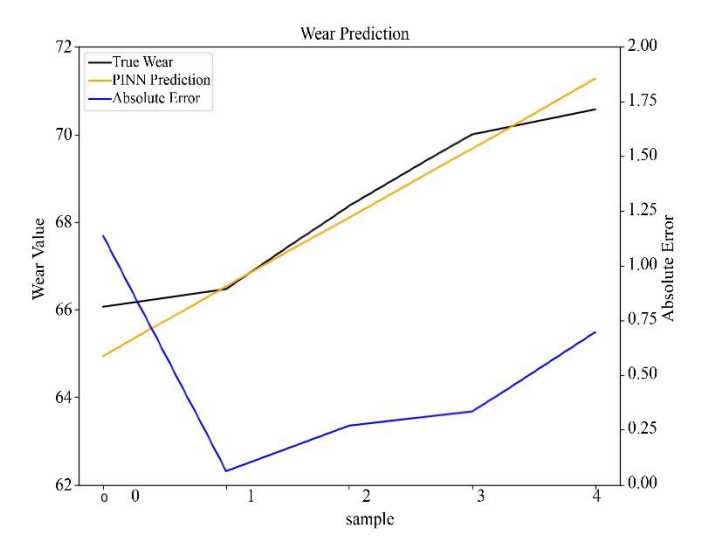
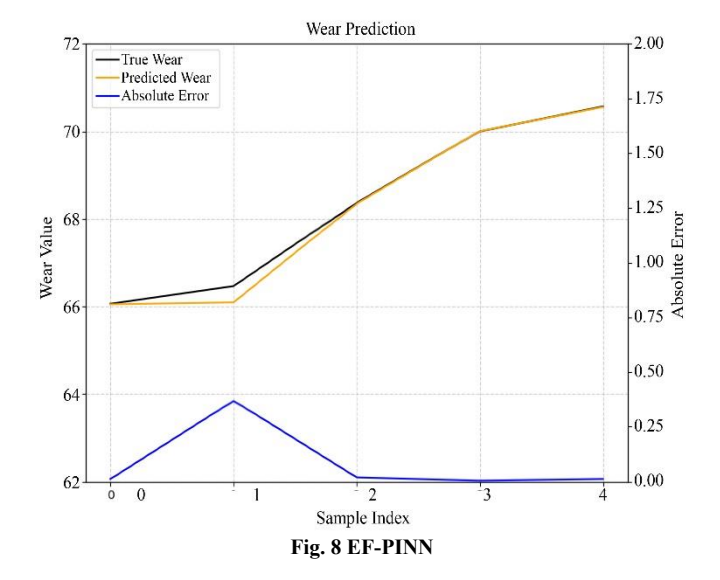


Fig. 7 Basquin-PINN



Analysis of PINN Model Prediction Results based on Empirical Formulations

As shown in Figure 8, the empirical formulation-based PINN model achieves an almost perfect match between the predicted wear curve (orange line) and the true wear curve (black line) across the entire wear process, with only a slight deviation observed at sample point 1. The overall prediction trend is highly consistent with the real wear evolution, and the absolute error (blue line) remains extremely low, indicating the superior accuracy and stability of the model.

This result demonstrates that embedding empirical physical relationships within the PINN framework effectively constrains the learning process, allowing the model to better capture the nonlinear dynamics of tool wear. Consequently, the empirical PINN model exhibits excellent generalization capability and strong robustness under complex working conditions, outperforming both the traditional LSTM and the Basquin-based PINN models.

5.4.2. Analysis of Experimental Results for Tool No. 5

As shown in the figures, the empirical formulation-based PINN model (Figure 11) demonstrates the best performance in tool wear prediction. Its absolute error remains close to zero (<0.1), with MAE below 0.05.

The predicted curve (yellow) almost perfectly overlaps with the true wear curve (black), with a correlation coefficient exceeding 0.99. In comparison, the LSTM model (Figure 9) exhibits large error fluctuations (0.2-1.5) and systematic

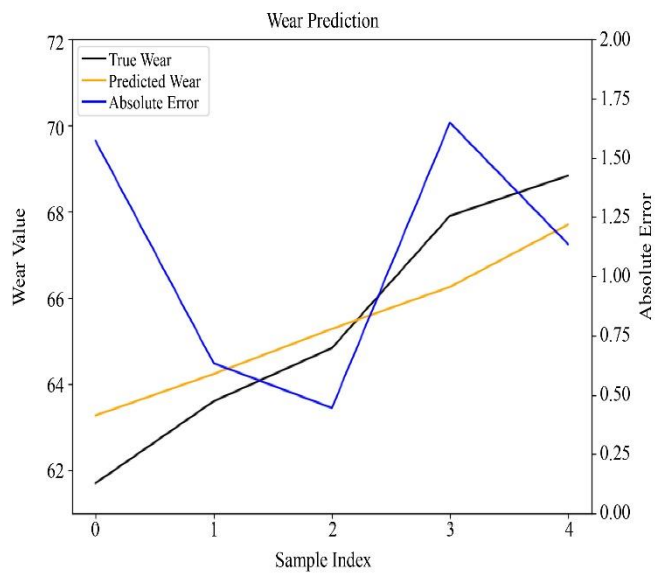
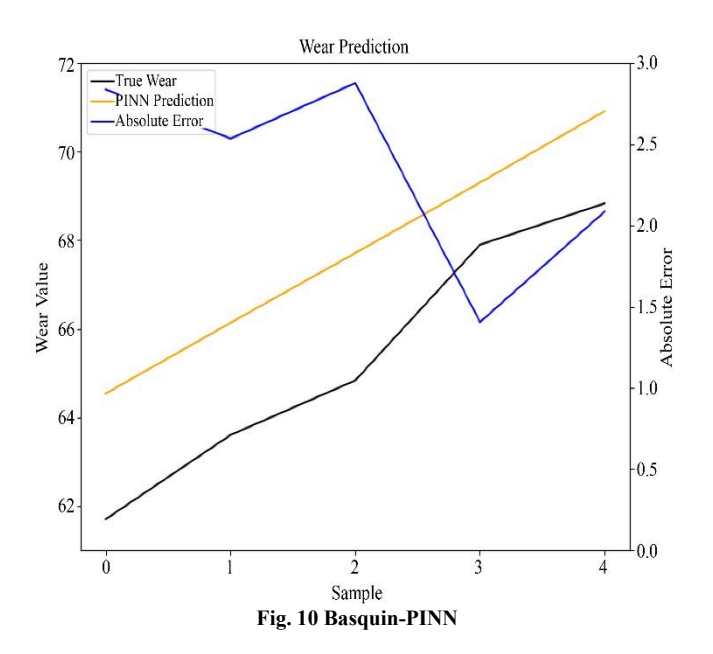


Fig. 9 Traditional neural network LSTM



deviations at multiple sample points, indicating poor prediction stability and generalization. The Basquin-PINN model (Figure 10) performs steadily in the mid-stage but shows an error peak of up to 0.8 in the later stage, revealing limitations of its physical constraints under accelerated wear.

Therefore, the empirical formulation-based PINN model achieves an effective synergy between physical knowledge and data-driven features, successfully enhancing the model's capability to capture complex wear mechanisms.

This result not only verifies the superior fitting performance shown in Figure 11 but also highlights the model's potential for interpretable and reliable tool wear prediction under real industrial conditions.

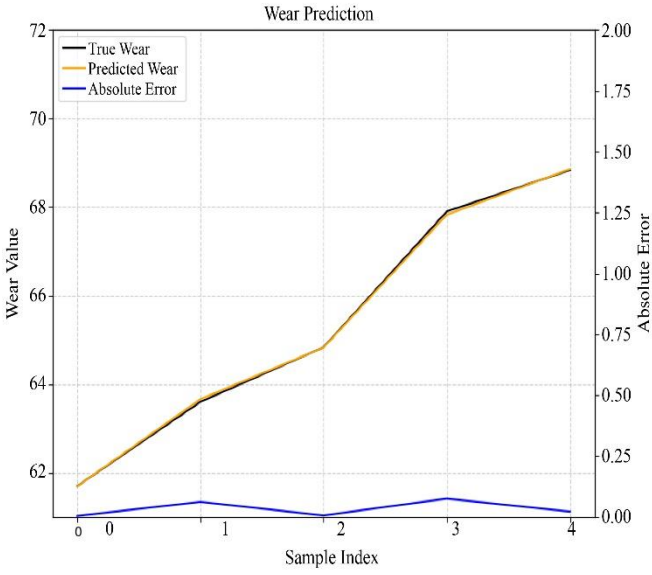


Fig. 11 EF-PINN

6. Conclusion

In this paper, three tool wear modeling methods are constructed based on the actual collected milling vibration signals, including traditional LSTM, the Basquin-PINN model, and the EF-PINN model. The key findings of this study are summarized as follows:

- 1. The empirical formula-driven PINN model performs optimally. Through the reasonable modelling of the wear evolution law and the efficient embedding of physical information, it achieves accurate fitting of the wear trend and exhibits excellent robustness and generalization in cross-tool tests. Moreover, it realizes an effective synergy between physical knowledge and data-driven learning, demonstrating strong adaptability to complex wear mechanisms and high potential for interpretable and reliable industrial applications.
- 2. The traditional LSTM model shows reasonable prediction capability in the initial and stable wear stages but fails to

- effectively respond to nonlinear variations during the accelerated wear phase. Its prediction error accumulates rapidly, leading to poor stability and generalization under complex conditions.
- The Basquin-based PINN model introduces physical constraints but lacks sufficient flexibility to represent the multi-stage nonlinear wear process, resulting in large fluctuations and limited overall prediction accuracy.

Subsequent research will focus on multimodal signal fusion and refined physical modelling to enhance the model's capability of describing and interpreting the wear evolution mechanism. In addition, incorporating uncertainty quantification and small-sample learning strategies will further improve its generalization and robustness under varying operating conditions.

Acknowledgement

This work was supported in part by the Key Research and Development (Major Scientific and Technological Innovation) Project of Shandong Province, China, under Grant No. 2019TSLH0202 and No. 2019JZZY01011, and in part by the Guangdong China Basic and Applied Basic Research Foundation under Grant No. 2021B1515120066.

Ethical Statement

All experiments were conducted in accordance with institutional ethical and safety standards. The datasets used in this study are open-source and released globally by the authors' research team, ensuring transparency and reproducibility. No human or animal subjects were involved, and all data collection followed ethical and data governance guidelines.

References

- [1] Luo Huan, Zhang Dinghua, and Luo Ming, "Tool Wear and Remaining Useful Life Estimation of Difficult-to-Machine Aerospace Alloys: A Review," *China Mechanical Engineering*, vol. 32, no. 22, pp. 2647-2666, 2021. [CrossRef] [Google Scholar] [Publisher Link]
- [2] P. Wan, Y.G. Li, and J.Q. Hua et al., "Accurate Prediction Method of Tool Wear Under Varying Cutting Conditions Based on Meta Learning and PINN," *Journal of Nanjing University of Aeronautics & Astronautics*, vol. 54, no. 3, pp. 387-396, 2022. [Google Scholar]
- [3] Y. Tian et al., "Multi-Objective Optimization of Machining Parameters Based on Tool Wear Condition," *Journal of Tianjin University* (science and Technology), vol. 55, no. 2, pp. 166-173, 2022. [Google Scholar]
- [4] Shi Keming et al., "A Multi Class Domain Adaptive Transfer Identification Method for Tool Wear States Under Different Processing Conditions," *China Mechanical Engineering*, vol. 33, no. 15, pp. 1841-1849, 2022. [CrossRef] [Google Scholar] [Publisher Link]
- [5] Changqing Liu et al., "A Meta-Invariant Feature Space Method for Accurate Tool Wear Prediction Under Cross Conditions," *IEEE Transactions on Industrial Informatics*, vol. 18, no. 2, pp. 922-931, 2022. [CrossRef] [Google Scholar] [Publisher Link]
- [6] Yiyuan Qin et al., "A Tool Wear Monitoring Method Based on Data-Driven and Physical Output," *Robotics and Computer-Integrated Manufacturing*, vol. 91, 2025. [CrossRef] [Google Scholar] [Publisher Link]
- [7] Kunpeng Zhu et al., "Physics-Informed Deep Learning for Tool Wear Monitoring," *IEEE Transactions on Industrial Informatics*, vol. 20, no. 1, pp. 524-533, 2024. [CrossRef] [Google Scholar] [Publisher Link]
- [8] Jinjiang Wang et al., "Physics Guided Neural Network for Machining Tool Wear Prediction," *Journal of Manufacturing Systems*, vol. 57, pp. 298-310, 2020. [CrossRef] [Google Scholar] [Publisher Link]
- [9] Hao Guo, Xin Lin, and Kunpeng Zhu, "Pyramid LSTM Network for Tool Condition Monitoring," *IEEE Transactions on Instrumentation and Measurement*, vol. 71, pp. 1-11, 2022. [CrossRef] [Google Scholar] [Publisher Link]
- [10] Minghui Cheng et al., "Intelligent Tool Wear Monitoring and Multi-Step Prediction Based on Deep Learning Model," *Journal of Manufacturing Systems*, vol. 62, pp. 286-300, 2022. [CrossRef] [Google Scholar] [Publisher Link]
- [11] Jing Zhang et al., "Remaining Life Prediction of Bearings Based on Improved IF-SCINet," *IEEE Access*, vol. 12, pp. 19598-19611, 2024. [CrossRef] [Google Scholar] [Publisher Link]
- [12] Linli Li, and Qifei Jian, "Remaining Useful Life Prediction of Wind Turbine Main-Bearing Based on LSTM Optimized Network," *IEEE Sensors Journal*, vol 24, no. 13, pp. 21143-21156, 2024. [CrossRef] [Google Scholar] [Publisher Link]
- [13] Dezhi Yuan et al., "The Cyber-Physical System of Machine Tool Monitoring: A Model-Driven Approach with Extended Kalman Filter Implementation," *IEEE Transactions on Industrial Informatics*, vol. 19, no. 9, pp. 9576-9585, 2023. [CrossRef] [Google Scholar] [Publisher Link]
- [14] Shenshen Li et al., "Physics-Guided Deep Learning Method for Tool Condition Monitoring in Smart Machining System," *IEEE/ASME Transactions on Mechatronics*, vol. 29, no. 3, pp. 2327-2337, 2024. [CrossRef] [Google Scholar] [Publisher Link]
- [15] Dezhi Yuan et al., "A Physics-Assisted Online Learning Method for Tool Wear Prediction," *IEEE Transactions on Instrumentation and Measurement*, vol. 72, pp. 1-11, 2023. [CrossRef] [Google Scholar] [Publisher Link]
- [16] Zepeng Liu et al., "Vibration Signal-Based Tool Condition Monitoring Using Regularized Sensor Data Modeling and Model Frequency Analysis," *IEEE Transactions on Instrumentation and Measurement*, vol. 73, pp. 1-13, 2024. [CrossRef] [Google Scholar] [Publisher Link]
- [17] Yafei Deng et al., "A Calibration-Based Hybrid Transfer Learning Framework for RUL Prediction of Rolling Bearing across Different Machines," *IEEE Transactions on Instrumentation and Measurement*, vol. 72, pp. 1-15, 2023. [CrossRef] [Google Scholar] [Publisher Link]

- [18] Yuekai Liu et al., "Physics-Informed Scaling Evolutionary Transformer for In-Situ Tool Condition Monitoring," *IEEE/ASME Transactions on Mechatronics*, vol. 29, no. 1, pp. 647-658, 2024. [CrossRef] [Google Scholar] [Publisher Link]
- [19] Xiaohui Fang et al., "A Dual Knowledge Embedded Hybrid Model Based on Augmented Data and Improved Loss Function for Tool Wear Monitoring," *Robotics and Computer-Integrated Manufacturing*, vol. 92, 2025. [CrossRef] [Google Scholar] [Publisher Link]
- [20] Haoyuan Zhang et al., "A Review of Physics-Based, Data-Driven, and Hybrid Models for Tool Wear Monitoring," *Machines*, vol. 12, no. 12, pp. 1-62, 2024. [CrossRef] [Google Scholar] [Publisher Link]
- [21] Chao Gao et al., "MPINet: Multiscale Physics-Informed Network for Bearing Fault Diagnosis with Small Samples," *IEEE Transactions on Industrial Informatics*, vol. 20, no. 12, pp. 14371-14380, 2024. [CrossRef] [Google Scholar] [Publisher Link]
- [22] Yejin Kim, and Young-Keun Kim, "Physics-Informed Time-Frequency Fusion Network with Attention for Noise-Robust Bearing Fault Diagnosis," *IEEE Access*, vol. 12, pp. 12517-12532, 2024. [CrossRef] [Google Scholar] [Publisher Link]
- [23] Yilin Li et al., "Physics-Informed Meta Learning for Machining Tool Wear Prediction," *Journal of Manufacturing Systems*, vol. 62, pp. 17-27, 2022. [CrossRef] [Google Scholar] [Publisher Link]
- [24] Chen Chong et al., "A Review of Physics-guided Deep Learning Research: Progress, Challenges and Prospects," *Computer Science and Exploration (CCF Chinese Category B)*, 2024. [Publisher Link]
- [25] Jiaqi Hua et al., "Physics-Informed Neural Networks with Weighted Losses by Uncertainty Evaluation for Accurate and Stable Prediction of Manufacturing Systems," *IEEE Transactions on Neural Networks and Learning Systems*, vol. 35, no. 8, pp. 11064-11076, 2024. [CrossRef] [Google Scholar] [Publisher Link]
- [26] Z. Sipos, "Investigation of Cutting Performance of Coated HSS Tools Made in Hungary," NME, Miskolc Egyetem, 1986. [Google Scholar]
- [27] General Administration of Quality Supervision, Inspection and Quarantine of the People's Republic of China, Chem Radar, Beijing, China, Asia, 2016. [Online]. Available: https://www.chemradar.com/lawinfo/authority/31
- [28] X. Li et al., "Fuzzy Neural Network Modelling for Tool Wear Estimation in Dry Milling Operation," *Annual Conference of the Prognostics and Health Management Society*, vol. 1, no. 1, pp. 1-11, 2009. [Google Scholar] [Publisher Link]